Effect of Reduced-Order Modelling on Passivity and Rendering Performance Analyses of Series Elastic Actuation

Kenanoglu, Celal Umut; Patoglu, Volkan

DOI
10.1109/LRA.2025.3561564

Publication date
2025

Document Version
Final published version

Published in
IEEE Robotics and Automation Letters

Effect of Reduced-Order Modelling on Passivity and Rendering Performance Analyses of Series Elastic Actuation

Celal Umut Kenanoglu, *Graduate Student Member, IEEE*, and Volkan Patoglu, *Member, IEEE*

***Abstract*—We study reduced-order models of series elastic actuation under velocity-sourced impedance control, where the inner motion controller is assumed to render the system into an ideal motion source within a control bandwidth and replaced by a low-pass filter. We present necessary and sufficient conditions for the passivity of this system and prove that the passivity results obtained through the reduced-order model may violate the passivity of the full-order model. To enable safe use of the reduced-order model, we derive conditions under which the passivity bounds of the reduced-order model guarantee the passivity of the full-order system. Moreover, we synthesize passive physical equivalents of closed-loop systems while rendering Kelvin-Voigt, linear spring, and null impedance models to provide rigorous comparisons of the passivity bounds and rendering performance among the full- and reduced-order models. We verify our results through a comprehensive set of simulations and experiments.**

***Index Terms*—Physical human-robot interaction, force control, compliance and impedance control, haptics and haptic interfaces, safety in HRI.**

I. Introduction

SERIES elastic actuation (SEA) is an interaction control approach introduced to provide safe and natural physical interactions that feature high stability robustness and rendering fidelity. SEA uses a linear compliant element intentionally introduced into mechanical design and relies on the model of this compliant element to implement closed-loop force control [1], [2], [3]. The existence of the compliant element not only improves contact stability by decreasing the reflected impedance of the plant as seen from the interaction port but also improves stability robustness by relaxing the stringent stability bounds on the controller gains that are imposed due to sensor-actuator non-collocation and actuator bandwidth restrictions [4], [5], [6]. Given that high rendering fidelity can only be achieved by actively compensating for the dynamics of the compliant element through its model, actuator saturation limits the performance bandwidth of SEA.

Series damped elastic actuation (SDEA) extends the control paradigm by adding a linear viscous dissipation element parallel to the spring of SEA [7], [8], [9], [10]. The addition of viscous dissipation to the series compliant element has been shown to help increase the force control bandwidth [7], reduce undesired oscillations [6], eliminate the need for derivative controller terms [9], and extend the upper limit on the passively renderable stiffness levels [10], [11].

The velocity-sourced impedance control (VSIC) is the most commonly used controller for SEA and SDEA (together abbreviated as S(D)EA), due to its reliable performance and ease of implementation [1], [3], [12], [13], [14]. The high performance of VSIC is mainly due to its inner motion control loop based on colocated sensor feedback [1]. Colocated sensor feedback enables high controller gains to be utilized in this motion control loop to effectively eliminate parasitic forces—undesired effects due to dissipation, compliance, and inertial dynamics that negatively affect the rendering performance—without inducing instability. Hence, the robust inner motion control loop can render the system to act as an ideal linear motion source within its control bandwidth, while the rest of the S(D)EA plant is intentionally designed to feature a linear time-invariant (LTI) series elastic element.

Given that S(D)EA under VSIC is designed as an LTI system, the coupled stability of interactions with this system has commonly been analyzed in the frequency domain. The coupled stability of interactions requires the system to be stable when attached to any passive environment. A necessary and sufficient condition to ensure the coupled stability of an LTI plant coupled to any passive environment is that the reflected impedance of the closed-loop plant as seen from the interaction port is passive. Consequently, the passivity of LTI systems ensures robust coupled stability across a wide range of environments, including those involving state-independent feedforward actions, such as non-malicious humans [15].

Passivity enables coupled stability analysis to be performed without the need for an environment model. Furthermore, the closed-form conditions derived from such analyses are of high value, as they offer analytical insights into the influence of system parameters on stability robustness. Passivity conditions are inherently robust as they restrict the phase of the closed-loop system to the right side of the complex plane, away from the critical point. However, there exists a fundamental trade-off in

Received 29 November 2024; accepted 30 March 2025. Date of publication 16 April 2025; date of current version 29 April 2025. This article was recommended for publication by Associate Editor K. Hashtrudi-Zaad and Editor J.-H. Ryu upon evaluation of the reviewers' comments. This work was supported by TUBITAK under Grant 23AG003. *(Corresponding author: Volkan Patoglu.)*

Celal Umut Kenanoglu is with the Department of Cognitive Robotics, Delft University of Technology, 2628 Delft, The Netherlands (e-mail: umut.kenanoglu@sabanciuniv.edu).

Volkan Patoglu is with the Faculty of Engineering and Natural Sciences, Sabanci University, Istanbul 34956, Türkiye (e-mail: volkan.patoglu@sabanciuniv.edu).

This article has supplementary downloadable material available at https://doi.org/10.1109/LRA.2025.3561564, provided by the authors.

Digital Object Identifier 10.1109/LRA.2025.3561564

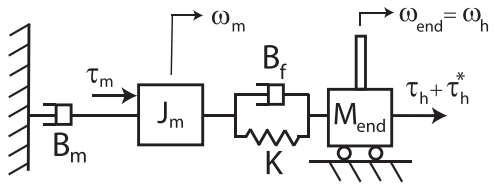

Fig. 1. Schematic representation of SDEA (SEA if $B_f = 0$).

interaction control between stability robustness and rendering performance [6], [11].

Under the assumption of a robust inner motion controller, reduced-order models have been used to study the passivity and rendering performance of SEA [16], [17], [18], [19]. For reduced-order modeling, the inner motion controller is assumed to render the system into an ideal motion source within a control bandwidth, while the physical interaction force applied to the actuator is further omitted.

Reduced-order modeling is valuable as such models enable more tractable closed-form analytical passivity conditions for complicated closed-loop systems, such as S(D)EA under VSIC. On the other hand, the performance and passivity conclusions obtained through such reduced-order models necessitate rigorous validation with respect to their corresponding full-order model, since, in general, there is no guarantee that these properties will match with that of the full-order model, as proven in Section V.

In this study, we rigorously analyze the consequences of reduced-order modeling on the coupled stability and haptic rendering performance of S(D)EA under VSIC. Our novel contributions can be listed as follows:

- We present necessary and sufficient conditions for the passivity of reduced-order models of S(D)EA under VSIC.
- We demonstrate that the passivity results obtained through the reduced-order model may violate the passivity of the full-order model.
- We derive conditions under which the passivity bounds of the reduced-order model guarantee the passivity of the full-order system.
- We introduce passive physical equivalents of reduced-order closed-loop systems while rendering Kelvin-Voigt (abbreviated as Voigt), spring, and null impedances.
- We provide rigorous comparisons of the passivity bounds and rendering performance among full- and reduced-order closed-loop systems.
- We present experimental verifications of our results.

II. Preliminaries

A schematic representation of a single-axis SDEA plant (without its controllers) is presented in Fig. 1. Without loss of generality, a rectilinear representation is used in the figures for simplicity of presentation, while all variables are kept in a rotary domain. Let J_m and B_m denote the reflected inertia and viscous damping of the actuator, including the reflected electrical damping. A physical compliant element consisting of a parallel torsional spring and viscous damper pair denoted by $K - B_f$, is placed between the end-effector and the actuator. Let the actuator and end-effector velocities be ω_m and ω_{end}. The symbol τ_m represents the actuator torque, while the end-effector inertia is denoted by M_{end}.

The interaction torque induced on the damped compliant element, also called the physical filter, is represented by τ_{sdea}. This interaction torque consists of the sum of the torques induced on the torsional spring and the viscous damper. Let τ_h and τ_h^* capture the human-induced torques on the system, which consists of a passive component τ_h and the deliberately applied active component τ_h^* which is assumed to be independent of the system states [15]. We assume that human interactions are non-malicious. The end-effector inertia of SDEA is neglected, so $\tau_{sdea}(s) \approx \tau_h + \tau_h^*$; hence, the impedance at the interaction port can be defined as $Z_{out}(s) = -\frac{\tau sdea(s)}{\omega_{end}(s)}$, where the spring-damper torque is considered as positive when these elements are in compression.

Fig. 2(a) illustrates the block diagram of the full-order model of SDEA under VSIC. The thick lines represent physical quantities, while G_t and G_m denote the torque and motion controllers, respectively. The colocated inner velocity control loop of VSIC effectively transforms the system into an ideal motion source. This loop operates on the motion reference signal ω_d generated by the outer torque control loop, whose aim is to regulate the spring-damper deflection at a desired level to match the reference force signal τ_d, computed according to the reference impedance Z_{ref}. The reference impedance is selected based on the impedance desired to be rendered at the interaction port [20].

The reduced-order modeling focuses on the colocated inner motion controller of S(D)EA under VSIC, highlighted in Fig. 2(a). It assumes that an aggressive and robust motion controller G_m renders this subsystem into an ideal motion source within a control bandwidth. The inner motion control loop of VSIC has the following transfer function:

$$\frac{\omega_m}{\omega_d} = \frac{G_m}{J_m s + B_m + G_m} = \frac{\frac{G_m}{J_m}}{s + \frac{B_m + G_m}{J_m}} = \gamma \frac{w_a}{s + w_a} \quad (1)$$

where $\gamma = \frac{G_m}{B_m + G_m}$.

Fig. 2(b) depicts the block diagram of the reduced-order model of S(D)EA under VSIC. The reduced-order model replaces the inner velocity loop with a first-order low-pass filter, where w_a captures the bandwidth of the motion-controlled subsystem in Fig. 2(a). In the reduced-order model, γ multiplies the torque controller gain, and for the simplicity of analysis, this scaled controller gain is redefined as G_t. In most practical cases, B_m is significantly smaller than G_m, resulting in $\gamma \approx 1$. Furthermore, the physical interaction force τ_{sdea} applied to the actuator as a disturbance is also omitted in the reduced-order model presented in Fig. 2(b), as it is assumed that this measured force can be partially canceled out with a feedforward control action and the motion-controlled system is designed to be sufficiently robust to compensate for the remaining disturbances.

III. Passivity of Reduced-Order Model

The impedance at the interaction port of the reduced-order model of SDEA under VSIC during Voigt model rendering is given by, $Z_{Voigt}^{SDEA_{red}}(s) = -\frac{\tau sdea(s)}{\omega_{end}(s)} =$

$$\frac{B_f\, s^3 + [K + B_f w_a (1 + B_{ref} G_t)]\, s^2 + [K\, w_a + G_t w_a (B_{ref} K + B_f\, K_{ref})]\, s + G_t\, K\, K_{ref}\, w_a}{s^3 + (w_a + B_f\, G_t\, w_a)\, s^2 + G_t\, K\, w_a\, s} \quad (2)$$

where the reference Voigt model is $Z_{ref} = \frac{K_{ref}}{s} + B_{ref}$ with K_{ref} and B_{ref} denoting respective spring and damping values.

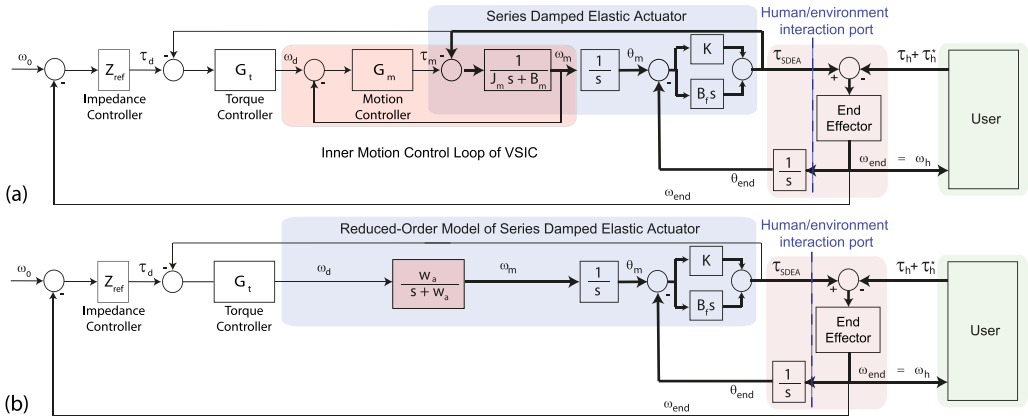

Fig. 2. Block diagrams of (a) full-order and (b) reduced-order models of S(D)EA under VSIC

Proposition 1: Consider the reduced-order model of Voigt model rendering with SDEA under VSIC as in Fig. 2(b), where G_t is a proportional gain. Let all parameters be positive. Then, the following expressions constitute necessary and sufficient conditions for the passivity of $Z_{Voigt}^{SDEA_{red}}(s)$.

i) $K \geq \frac{K_{ref}}{B_{ref}\,G_t+1}$, and

ii) $-\frac{2\sqrt{B_f G_t K(K-K_{ref}+B_{ref}G_t K)}-G_t(B_{ref}K+B_f K_{ref})}{B_f(B_{ref}G_t+1)(B_f G_t+1)} \leq w_a$

The proof is presented in Appendix A.

For a simpler set of *sufficient* conditions, Condition (ii) of Proposition 1 can be replaced by the following:

$$\frac{G_t\,(B_{ref}\,K+B_f\,K_{ref})}{B_f\,(B_{ref}\,G_t+1)\,(B_f\,G_t+1)} \leq w_a \tag{3}$$

The impedance at the interaction port of the reduced-order model of SDEA under VSIC during Voigt model rendering given in (2) reduces to that of SEA under VSIC during Voigt model rendering when B_f is zero.

Corollary 1: Consider the reduced-order model of Voigt model rendering with SEA under VSIC in Fig. 2(b), where $B_f = 0$ and G_t is a proportional gain. Let all parameters, except B_{ref}, be positive. Then, the following expressions constitute necessary and sufficient conditions for the passivity of $Z_{Voigt}^{SEA_{red}}(s)$.

i) $0 < K_{ref} \leq (B_{ref}G_t+1)K$, and

ii) $-1 \leq B_{ref}G_t \leq 0$.

The proof follows from Proposition 1 by setting $B_f = 0$.

Note that passive Voigt model rendering with SEA under VSIC is only possible when $B_{ref} \leq 0$, indicating that while the physical damping in the system can be compensated, augmentation of system damping is not possible with SEA under VSIC under the passivity constraints.

Remark 1: When B_{ref} (B_{ref} and K_{ref}) is set to zero in (2), the output impedance transfer function for SDEA becomes equal to the transfer function for spring (null impedance) rendering. Accordingly, necessary and sufficient conditions for spring rendering with SDEA reduce to Conditions (i) and (ii) of Proposition 1 with $B_{ref}=0$ ($B_{ref}=K_{ref}=0$). During null impedance rendering, Conditions (i) and (ii) of Proposition 1 are always satisfied.

Similarly, the output impedance transfer function and the necessary and sufficient conditions for spring and null impedance rendering with SEA can be derived by substituting $B_f = B_{ref}=0$ and $B_f=B_{ref}=K_{ref}=0$ into (2) and Corollary 1, respectively.

IV. Analysis of Rendering Performance of S(D)EA$_{red}$ via Passive Physical Equivalents

Passive physical equivalents (also called realizations) describe physically realizable behaviors with a network of passive fundamental elements in a domain to realize a driving-point impedance. Realizations are useful as they provide analytical insights into the trade-offs between passivity and performance in interaction controllers and facilitate rigorous comparisons of various plant and controller dynamics with each other [6], [20], [21].

Passive physical equivalents not only provide sufficient conditions for passivity but also establish an intuitive understanding of these bounds in terms of the non-negativity of fundamental mechanical elements involved in their topology. Moreover, these realizations explicitly demonstrate how plant parameters and controller gains influence rendering performance; they clarify the extent of controller authority on the closed-loop system and enable the rendered dynamics to be distinguished from the parasitic terms. Accordingly, one can analytically study the fundamental passivity-performance trade-offs due to plant and controller parameters through realizations. Furthermore, they offer a structured analytical framework for rigorous comparisons of various closed-loop dynamics resulting from different system configurations. In this study, we utilize passive physical equivalents for analytical comparisons of full- and reduced-order systems.

A. Passive Physical Equivalent of SDEA$_{red}$

A realization of the impedance at the interaction port as in (2), characterizing the reduced-order model of SDEA under VSIC during Voigt model rendering when the controller is proportional, is presented in Fig. 3(a). The parameters of this realization are given as: $c_{1v} = \frac{K-K_{ref}}{G_t\,K}$, $b_{1v} = \frac{B_f-B_{ref}}{B_f\,G_t\,w_a}$, $c_{2v} = \frac{(B_f\,K_{ref}-B_{ref}\,K)\,(B_f\,w_a-K)}{{B_f}^2\,G_t\,K\,w_a}$, and $b_{2v} = \frac{(B_f\,K_{ref}-B_{ref}\,K)\,(B_f\,w_a-K)}{B_f\,G_t\,K^2\,w_a}$.

For the realization in Fig. 3(a) to be feasible, all components should be non-negative. Hence, the non-negativeness of the terms imposes:

$$K \geq K_{ref} \text{ and } B_f \geq B_{ref} \text{ and } w_a \geq \frac{K}{B_f} \text{ and } \frac{B_f}{K} \geq \frac{B_{ref}}{K_{ref}} \tag{4}$$

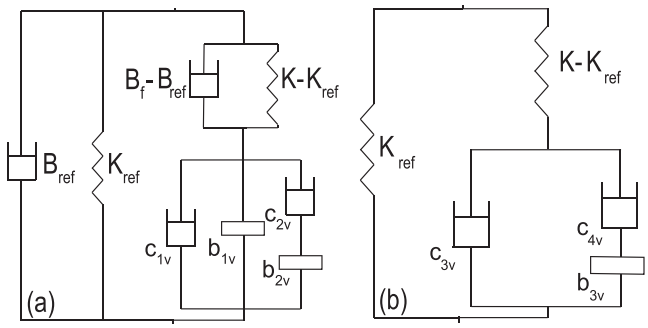

Fig. 3. The passive physical equivalents of the reduced-order models of the Voigt rendering under VSIC of plants with (a) SDEA (for $B_{ref} \geq 0$) and (b) SEA (for $B_{ref} \leq 0$).

These conditions impose constraints that are more conservative than Condition (i) of Proposition 1 and (3). Consequently, the feasibility of Fig. 3(a) provides sufficient conditions for the passivity of (2). Physical realization of the reduced-order model of SDEA under VSIC during Voigt model rendering in Fig. 3(a) consists of three main branches in parallel: a spring-damper pair K_{ref}–B_{ref} in parallel, and a branch capturing the parasitic dynamics governed by a complex topology of damper-inertance terms (c_{1v}, c_{2v}, b_{1v}, and b_{2v}) that are coupled to the system in series through a coupling filter. This coupling filter also consists of a spring-damper pair in parallel, where the stiffness and damping of the filter are given by $K - K_{ref}$ and $B_f - B_{ref}$, respectively.

The parasitic dissipation effects are split into two parts: a damper term (c_{1v}) multiplied by $\frac{1}{G_t}$ indicating a significant effect of the force control gain G_t on this damper term, and a serial damper-inerter term (c_{2v} - b_{2v}) that introduces frequency-dependent dissipation to the system that increases with frequency. The parasitic inertance (b_{1v}) reduces with higher force control gain G_t like the damper term. Furthermore, this inertance is scaled with $\frac{1}{w_a}$, indicating that a higher cut-off frequency reduces the parasitic inertance.

After removing the rendered Voigt model K_{ref} -B_{ref} and the serial coupling filter $(B_f - B_{ref})$–$(K - K_{ref})$ pairs, the effective damping of Fig. 3(a) can be computed as

$$\frac{[B_f(B_f-B_{ref})w_a+B_{ref}K-B_fK_{ref}]w^2+K(K-K_{ref})w_a}{\left(B_f{}^2G_tw_a\right)w^2+G_tK^2w_a} \tag{5}$$

which converges to c_{1v} at low frequencies, while it approaches to $c_{1v} + c_{2v}$ at high frequencies. Similarly, the effective inertance of the subsystem can be computed as

$$\frac{[B_f(B_f-B_{ref})]w^2+K(K-K_{ref})-(B_{ref}K-B_fK_{ref})w_a}{\left(B_f{}^2G_tw_a\right)w^2+G_tK^2w_a} \tag{6}$$

which converges to $b_{1v} + b_{2v}$ at low frequencies, while it approaches to b_{1v} at high frequencies.

B. Passive Physical Equivalent of SEA$_{red}$

A realization of the reduced-order model of SEA under VSIC during Voigt model rendering when the controller is proportional is presented in Fig. 3(b). The parameters of this realization are given as: $c_{3v} = B_{ref} + \frac{K-K_{ref}}{G_t K}$, $b_{3v} = \frac{B_{ref}{}^2}{K-K_{ref}} + \frac{K-K_{ref}+B_{ref}w_a}{G_t K w_a}$, and $c_{4v} = -B_{ref} - \frac{(K-K_{ref})(K-K_{ref}+B_{ref}w_a)}{B_{ref}G_tKw_a}$.

Note that this realization is significantly different from the realization in Fig. 3(b), since passive Voigt model rendering with SEA under VSIC is only possible for $B_{ref} \leq 0$.

For the realization in Fig. 3(b) to be feasible, all components should be non-negative. Non-negativeness of c_{3v} imposes Condition (i) of Corollary 1. Moreover, if we substitute the non-negativeness condition of c_{3v} into b_{3v} and c_{4v}, we observe that B_{ref} should be negative for non-negativeness of b_{3v} and c_{4v}. Hence, the feasibility of the realization provides sufficient conditions for the passivity of the system. Accordingly, if we consider that the controller gains are positive, then the realization is valid as long as B_{ref} is negative, and Condition (i) of Corollary 1 are satisfied with non-negative b_{3v} and c_{4v} values.

Fig. 3(b) indicates two main branches in parallel: a spring K_{ref}, and a branch capturing the parasitic dynamics and desired damping value governed by a complex topology of damper-inertance terms (c_{3v}, c_{4v}, and b_{3v}) that are coupled to the system in series through a coupling spring with a stiffness of $K - K_{ref}$.

The low-frequency damping behavior of this realization is captured by c_{3v}, which is adjustable via B_{ref}. When a high value of G_t is chosen, the value of c_{3v} converges to B_{ref} at low frequencies, demonstrating that the damping in the system approaches B_{ref}. It is important to remember the trade-off; since the passivity constraint requires B_{ref} to be negative, while the feasibility of the realization requires c_{3v} not to be negative.

After removing the rendered virtual stiffness K_{ref} and the serial coupling filter $K - K_{ref}$ from the system, the effective damping of the realization in Fig. 3(b) becomes (7) shown at the bottom of the next page which converges to c_{3v} at low frequencies, while it approaches to c_{3v}+c_{4v} at high frequencies. Similarly, the effective inertance of the realization in Fig. 3(b) is (8) shown at the bottom of the next page which converges to b_{3v} at low frequencies, while it approaches zero at high frequencies.

When the realizations of the reduced-order models are compared with those of the corresponding full-order in [20], it can be observed that both the structure and the behavior of the realizations are quite similar to each other. Furthermore, the reduced-order model captures the similar stability-performance trade-offs as the full-order model, while resulting in realizations that are easier to interpret. Numerical comparisons are presented in Section VI.

Remark 2: When $B_{ref} = 0$ ($B_{ref} = K_{ref} = 0$), Fig. 3(a) reduces to the passive physical equivalent of linear spring rendering (null impedance) rendering with SDEA. Similarly, the passive physical equivalent of linear spring (null impedance) rendering with SEA can derived from Fig. 3(b) by substituting $B_{ref} = 0$ ($B_{ref} = K_{ref} = 0$).

V. Passivity of Reduced vs Full-Order Model

The results of Section III indicate that the passivity results obtained through the reduced-order model may violate the passivity of the full-order model. Below, we present the conditions under which the passivity bounds of the reduced-order model guarantee the passivity of the full-order system, to enable safe use of the reduced-order model.

Proposition 2: Consider positive controller parameters for Voigt model rendering with S(D)EA, with the exception of negative B_{ref} for SEA. The necessary and sufficient conditions

TABLE I
PARAMETERS OF THE SDEA PLANT IN SIMULATIONS

Parameter	Value	Parameter	Value
J_m	0.002 kgm^2	B_m	0.18 Nms/rad
K	360 Nm/rad	B_f	0.15 Nms/rad

of the reduced-order model S(D)EA$_{red}$ with $w_a \triangleq \frac{B_m+G_m}{J_m}$ to ensure the passivity of the full-order model of S(D)EA under VSIC are as follows:

(i) $B_{ref}(1 - B_m G_t) \geq 0$ or

(ii) $B_{ref}(1 - B_m G_t) < 0$ and $\frac{B_{ref} G_m G_t (B_m G_t - 1)}{J_m} \leq w_a$.

The proof is presented in Appendix B. Note that, while B_{ref} is positive for SDEA, it must be negative for SEA.

In Condition (i), $1 - B_m G_t \geq 0$ term ensures that the damping term c_{1v} in the realization of the reduced-order model in Fig. 3(a) underestimates the corresponding damping term in the realization of the full-order model of SDEA under VSIC during Voigt model rendering [20], since this damping term dominates the parasitic dynamics at low frequencies and the effective damping of both reduced- and full-order models converge to B_f at high frequencies. Furthermore, since B_{ref} must be negative for SEA during Voigt model rendering, the sign of the condition is reversed accordingly.

Similarly, Condition (ii) ensures that the effective damping of the overall realization of the reduced-order model does not overestimate that of the full-order system.

Remark 3: The passivity of the reduced-order model with $w_a = \frac{B_m+G_m}{J_m}$ provides a sufficient condition for the passivity of the full-order system during spring rendering. Furthermore, null impedance rendering with the reduced- and full-order models is always passive for S(D)EA, if non-negative controller gains are utilized.

VI. NUMERICAL EVALUATIONS

Table I presents the SDEA plant parameters used for the numerical simulation, while the controller gains are selected as $G_t = 5$ rad/sNm and $G_m = 5$ Nms/rad. These parameters are selected so that a clear counterexample can be provided to support the theoretical analysis.

Fig. 4(a) presents Bode plots of reduced- and full-order models while rendering Voigt models with $B_{ref} = 0.05$ Nms/rad. The passivity of these systems can be easily visualized from the Bode phase plots, as the phase is restricted to stay within the $[-\frac{\pi}{2}, \frac{\pi}{2}]$ range for passive systems. The figure shows that the reduced- and full-order models are both passive when $K_{ref} = 150$ Nm/rad. Similarly, the reduced- and full-order models are both active when $K_{ref} = 600$ Nm/rad. However, when $K_{ref} = 455$ Nm/rad, the full-order model remains passive, whereas the reduced-order model no longer maintains its passivity. In this case, the reduced-order model provides a more conservative bound than the full-order model, as $1 - B_m G_t \geq 0$.

Conversely, Fig. 4(b) illustrates two scenarios when $1 - B_m G_t < 0$. In particular, the condition $\frac{B_{ref} G_m G_t (B_m G_t - 1)}{J_m} \leq w_a$ is not met for $G_t = 15$ rad/sNm and $K_{ref} = 630$ Nm/rad and the full-order model becomes more conservative than the reduced-order model. This implies that, under these controller parameters, the passivity of the reduced-order model cannot guarantee the passivity of the full-order model. In contrast, when $G_t = 10$ rad/sNm and $K_{ref} = 542$ Nm/rad, $\frac{B_{ref} G_m G_t (B_m G_t - 1)}{J_m} \leq w_a$ is satisfied, confirming that the reduced-order model still provides a more conservative bound than the full-order model.

Fig. 4(c) presents the effective damping and effective spring of the reduced- and full-order models, respectively. In these figures, $K_{ref} = 150$ Nm/rad, while $B_{ref} = 0.05$ Nms/rad for SDEA and $B_{ref} = -0.05$ Nms/rad for SEA. Fig. 4(c) shows that the effective damping of the reduced-order model underestimates the effective damping of the full-order model, as required by the passivity condition $(B_{ref}(1 - B_m G_t) \geq 0)$. At low frequencies, the effective damping converges to $c_{1v} + B_{ref}$ for SDEA and c_{3v} for SEA, as shown by their respective passive physical equivalents.

Similarly, Fig. 4(c) indicates that the effective stiffness is $K_{ref} = 150$ Nm/rad for both SEA and SDEA for the reduced-order model, while the effective stiffness of the full-order model is $\frac{G_m G_t}{G_m G_t + 1} K_{ref}$ in the low-frequency range, which is also consistent with their respective passive realizations.

Numerical effective impedance comparisons in Fig. 4(c) show that the performance of the reduced- and full-order models are quite close to each other, and the reduced-order realizations can be used to study the performance trade-offs involved in the full-order system, as predicted in Section IV.

VII. EXPERIMENTAL VALIDATION

This section validates the theoretical passivity limits of the reduced-order model of S(D)EA through physical experiments. We employ a modified version of the single-axis SEA brake pedal depicted in Fig. 5(a) [22]. The SEA brake pedal is driven by a brushless DC motor equipped with a Hall-effect sensor and an optical encoder. Motor torque is amplified with a transmission ratio of 1:39.5. The series elastic component is implemented as a compliant cross-flexure joint whose deflections are measured with a linear encoder to estimate interaction torques. The system is controlled in real-time at 1 kHz via an industrial PC connected to an EtherCAT bus. For the SDEA implementation, the system is augmented with an eddy-current damper in parallel to the cross-flexure joint. Furthermore, the stiffness of the cross-flexure

$$-\frac{\left[B_{ref}(K-K_{ref})^2\right] w^2+\left[(K-K_{ref})^3+B_{ref}G_tK(K-K_{ref})^2\right] w_a}{\left(B_{ref}^2 G_t K w_a\right) w^2 + G_t w_a K (K-K_{ref})^2} \tag{7}$$

$$\frac{G_t w_a B_{ref}^2 K(K-K_{ref}) + w_a B_{ref}(K-K_{ref})^2 + (K-K_{ref})^3}{(G_t w_a B_{ref}^2 K) w^2 + G_t w_a K (K-K_{ref})^2} \tag{8}$$

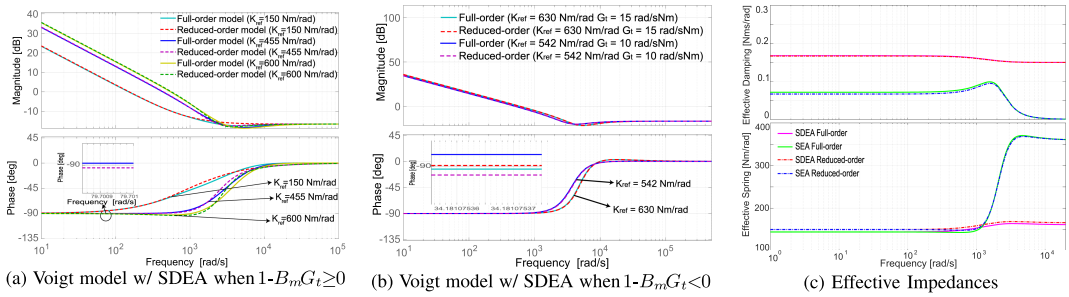

(a) Voigt model w/ SDEA when $1\text{-}B_m G_t \geq 0$ (b) Voigt model w/ SDEA when $1\text{-}B_m G_t < 0$ (c) Effective Impedances

Fig. 4. (a)–(b) Bode plots comparing the passivity of full-order and reduced-order models during Voigt model rendering, and (c) effective impedance analysis of full-order and reduced-order models for S(D)EA to show the similarity of performances.

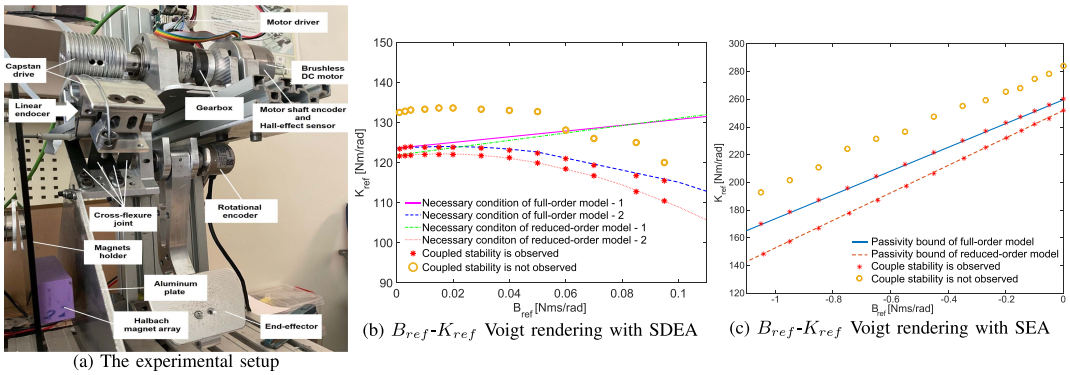

(a) The experimental setup (b) B_{ref}-K_{ref} Voigt rendering with SDEA (c) B_{ref}-K_{ref} Voigt rendering with SEA

Fig. 5. The S(D)EA pedal (a) and results of coupled stability experiments during Voigt rendering with (b) SDEA and (c) SEA.

TABLE II
PARAMETERS OF THE S(D)EA PLANT

Parameter	Value	Unit
J_m	0.0024	kgm^2
B_m	0.0177	Nms/rad
K	121.8 (for SDEA) and 252 (for SEA)	Nm/rad
B_f	0.0127	Nms/rad

joint is reduced by half for the SDEA implementation to ensure a larger effect of B_f with respect to K.

The experimentally determined plant parameters are presented in Table II [20]. Nominal VSIC controller gains are set to $G_m = 0.0576$ Nms/rad and $G_t = 30$ rad/(sNm).

Theoretical passivity bounds in the previous sections are derived assuming a unity reduction ratio in power transmission. These results generalize to system with a reduction ratio n through the following mappings: $J_{m_{eq}} = n^2\, J_m$, $B_{m_{eq}} = n^2\, B_m$, $G_{m_{eq}} = n^2\, G_m$, and $G_{t_{eq}} = 1/n\, G_t$.

A. *Verification of Passivity Bounds*

We investigate the passivity of the system by studying the stability of interactions when coupled to the most destabilizing environments. The passivity is affirmed only if no set of ideal springs or inertias destabilizes the system under excitations spanning all frequencies. Inertial environments are the most destabilizing environments for S(D)EA.

The S(D)EA brake pedal under VSIC was connected to various inertias and impacts were imposed to its end-effector. Non-passivity conclusions were made if any violation of the coupled stability was observed. Conversely, if no violations were detected during multiple trials with gradual increase in the end-effector inertia, it was concluded that experimental evidence supports passivity. A video of sample experiments is provided in the Multimedia Extension.

Voigt Model Rendering with SDEA: In these experiments, we studied the coupled stability of SDEA under VSIC during Voigt rendering. A line search was conducted along the K_{ref} values for different B_{ref} values, starting from 25% below the most conservative theoretical passivity bound, while K_{vir} was increased with a resolution of 0.5 Nm/rad. The necessary and sufficient conditions of the full-order model were utilized as in [20]. The conditions for the reduced-order model were calculated from Conditions (i) and (ii) of Proposition 1. Fig. 5(b) shows that one of the conditions of the reduced-order model presents a more conservative bound than the corresponding condition of the full-order model for all B_{ref}. On the other hand, the second condition of the reduced-order model presents a more conservative bound than the full-order model until $B_{ref} \approx 0.0862$ Nms/rad, after which (16) is violated.

Fig. 5(b) presents the experimental K_{ref}–B_{ref} plot for the SDEA brake pedal. In the figure, the necessary and sufficient conditions of full-order model are depicted as the magenta and blue lines. In the figure, the theoretical passivity bound according to Condition (i) of Proposition 1 is depicted as the green line, while the bound according to Condition (ii) of Proposition 1 is depicted as the orange line. The experimental results validate the analytically predicted passivity boundary. In particular, experimental results follow the dashed blue line which is the stricter condition. The theoretical bounds are about 8% more conservative, as the physical system is likely to have some extra dissipation.

Voigt Model Rendering with SEA: In these experiments, we studied the coupled stability of SEA under VSIC during Voigt model rendering. We tested various K_{ref} and B_{ref} values when $G_t = 15$ rad/(sNm). The necessary and sufficient condition for

the full-order model is computed from [20], while the passivity condition for the reduced-order model is computed from Corollary 1.

Fig. 5(c) presents the experimental K_{ref}–B_{ref} plot for the SEA brake pedal. In Fig. 5(c), the passivity conditions according to the full- and reduced-order models are presented as the blue and orange dashed lines, respectively. The figure indicates that the passivity of the reduced-order model provides a sufficient condition for the full-order model. The theoretical bounds are about 8% more conservative.

We have also investigated the coupled stability of both SDEA and SEA under VSIC during spring rendering, that is, when $B_{ref} = 0$ during Voigt model rendering. For each case, we analyzed the range of K_{ref} values for different G_t gains based on the necessary and sufficient conditions. Our experimental results (not shown due to space restrictions) validate the analytically predicted passivity boundaries and demonstrate the conservativeness of the reduced-order model. The theoretical bounds for SDEA and SEA were about 6.5% more conservative than the experimental results.

VIII. Conclusion

Reduced-order modeling relies on good velocity tracking performance of the inner motion control subsystem within a performance bandwidth. Since the existence of a robust collocated control loop around the actuator is one of the key underlying ideas of the S(D)EA paradigm [1], this assumption remains valid for most systems with S(D)EA and is independent of the controller employed to achieve this goal. Furthermore, the robust control of the actuator and the linearity of the intentionally designed series elastic element enable systems with S(D)EA possess linear dynamics, allowing them to be particularly suitable for LTI analysis.

The reduced-order model is commonly employed as it enables easier analysis; however, the results of such analyses must be validated against the full-order model. We have provided necessary and sufficient conditions for the passivity of the reduced-order model of S(D)EA under VSIC. Our analysis has revealed instances where the passivity results obtained from the reduced-order model may not align with those of the full-order model of SDEA. Consequently, we have derived conditions under which the passivity bounds of the reduced-order model ensure the passivity of the full-order system. Specifically, if the product of the viscous damping of the actuator and the torque controller gain exceeds one for SDEA, the parameter w_a should be selected higher than $\frac{B_{ref} G_m G_t (B_m G_t - 1)}{J_m}$. Conversely, if this product is less than one for SEA, w_a should be higher than the same limit.

We have introduced passive physical equivalents for the reduced-order model while rendering Voigt, spring, and null impedance. These passive physical equivalents not only enable explicit study of the rendered impedance and parasitic dynamics but also facilitate objective comparisons among reduced- and full-order models in terms of their rendering performance. Additionally, we have presented rigorous comparisons of passivity bounds and rendering performance across different closed-loop systems utilizing the full- and reduced-order models. Our results indicate that both the structure and the behavior of the reduced- and full-order realizations are quite similar to each other. Moreover, the reduced-order model captures the similar stability-performance trade-offs as the full-order model. Accordingly, by employing the passivity guarantees provided in Proposition 2, the reduced-order models can be used to effectively study S(D)EA under VSIC.

Our future work includes extending this analysis to various controllers, including model reference force controller [23]. Extending the S(D)EA paradigm to systems with multiple degrees of freedom and/or with non-linear series elastic elements are other possible interesting research directions.

Appendix A

Proof: According to the positive realness theorem [15], [24], the necessary and sufficient conditions are:

1) $Z(s)$ has no poles in the right half plane. $Z_{Voigt}^{SDEA_{red}}(s)$ has no roots in the open right half plane if all coefficients of denominator of $Z_{Voigt}^{SDEA_{red}}(s)$ are positive.

2) $Re[Z(jw)] \geq 0$ for all w. The sign of $Re[Z_{Voigt}^{SDEA_{red}}(jw)]$ can be checked by the sign of $H(jw) = d_6 w^6 + d_4 w^4 + d_2 w^2$ where

$$d_2 = G_t\, K\, {w_a}^2\, (K - K_{ref} + B_{ref}\, G_t\, K) \tag{9}$$

$$d_4 = B_f {w_a}^2 (B_{ref} G_t + 1)(B_f G_t + 1) - B_{ref} G_t K w_a - B_f G_t K_{ref} w_a \tag{10}$$

$$d_6 = B_f \tag{11}$$

The coefficient d_6 is always positive, since B_f is positive. Non-negativeness of d_2 imposes Condition (i) of Proposition 1. The last necessary and sufficient condition can be derived from the condition $d_4 \geq -2\sqrt{d_2 d_6}$ as the Condition (ii) of Proposition 1.

3) Any poles of Z(s) on the imaginary axis are simple with positive and real residues. There exists no poles on the imaginary axis, except at $s = 0$, when all controller gains and w_a are positive. When $s = 0$, the residue equals to K_{ref}, which is always positive and real for positive K_{ref}. ■

Appendix B

Proof: Equations (12) and (13) present the passivity conditions for Voigt model rendering of the full-order model for SDEA under VSIC when the controller gains are positive [20], where (12) is a necessity condition, while (13) is a sufficient condition for Voigt model rendering with the full-order SDEA model.

$$K \geq K_{ref}\, \frac{\alpha}{(\alpha + 1)}\, \frac{B_m + G_m}{B_m + G_m + B_{ref}\, \alpha} \tag{12}$$

$$J_m \leq \frac{B_f\, (B_m + G_m + B_{ref}\, \alpha)\, [B_m + G_m + B_f\, (1 + \alpha)]}{(B_f\, K_{ref} + B_{ref}\, K)\, \alpha} \tag{13}$$

where $\alpha = G_m G_t$. When the necessary conditions presented in Condition (i) of Proposition 1 and (12) are compared:

$$K \geq \frac{K_{ref}}{B_{ref}\, G_t + 1} \geq K_{ref}\, \frac{\alpha}{(\alpha + 1)}\, \frac{B_m + G_m}{B_m + G_m + B_{ref}\, \alpha} \tag{14}$$

Accordingly, (14) shows that SDEA_{red} presents a more conservative bound than SDEA when the following equation holds:

$$0 \leq B_m + G_m + B_{ref}\, \alpha\, (1 - B_m G_t) \tag{15}$$

Since $w_a = \frac{B_m+G_m}{J_m}$, (15) can be rearranged as:

$$w_a \geq \frac{B_{ref}\,\alpha\,(B_m G_t - 1)}{J_m} \tag{16}$$

If $1 - B_m G_t \geq 0$, then there is no need to check (15) or (16), and (14) always holds. If $1 - B_m G_t < 0$ and the cut-off frequency of the reduced-order model is selected to satisfy (16), then it can be shown that the passivity bound of SDEA$_{red}$ in Condition (i) of Proposition 1 provides a sufficient condition for the passivity bound of SDEA in (12). In particular, the comparison of the sufficient conditions presented in (3) and (13) indicate that

$$\begin{aligned} J_m &\leq \frac{B_f(B_{ref}G_t+1)(B_f G_t+1)(B_m+G_m)}{(B_f\,K_{ref}+B_{ref}\,K)\;G_t} \\ &\leq \frac{B_f\;(B_m+G_m+B_{ref}\,\alpha)\,[B_m+G_m+B_f\,(1+\alpha)]}{(B_f\,K_{ref}+B_{ref}\,K)\;\alpha} \end{aligned} \tag{17}$$

Equation (3) presents a more conservative bound than (13) if the following relation holds:

$$0 \leq B_{ref}\,B_f\,\alpha\,(1 - B_m G_t) + (B_m + G_m)(B_m + B_f) \tag{18}$$

Since $w_a = \frac{B_m+G_m}{J_m}$, (18) can be rearranged as:

$$w_a \geq \frac{B_{ref}\,B_f\,\alpha\,(B_m G_t - 1)}{J_m(B_m + B_f)} \tag{19}$$

If $1 - B_m G_t \geq 0$, then there is no need to check (18) or (19), and (17) always holds. If $1 - B_m G_t < 0$, then the passivity bound of SDEA in (13) is ensured when (19) is satisfied. However, (16) presents a more conservative bounds than (19).

Similarly, for Voigt model rendering with SEA under VSIC, (20) and (21) provide the necessary and sufficient conditions for the passivity of the full-order model of SEA under VSIC when controller gains, except B_{ref}, are positive [20].

$$\frac{\alpha}{\alpha+1}\,K_{ref} \leq \left(1 + \frac{\alpha\,B_{ref}}{B_m+G_m}\right) K \tag{20}$$

$$-\,(B_m+G_m) \leq \alpha\,B_{ref} \;\leq\; 0 \tag{21}$$

A comparison of (20) with Corollary 1 indicates (14). Accordingly, (14) shows that the reduced-order model SEA$_{red}$ presents more conservative bounds than the full-order model of SEA if (15) or (16) is satisfied for $B_{ref} \leq 0$. If Condition (ii) of Corollary 1 and (21) are compared, then Condition (ii) of Corollary 1 is always more conservative than (21), since $B_m > 0$. ■

ACKNOWLEDGMENT

Kenanoglu's work was carried out during his graduate studies at Sabanci University.

REFERENCES

[1] R. D. Howard, "Joint and actuator design for enhanced stability in robotic force control," Ph.D. dissertation, Massachusetts Institute of Technology, Cambridge, MA, USA 1990.

[2] G. A. Pratt and M. M. Williamson, "Series elastic actuators," in *Proc. IEEE/RSJ Int. Conf. Intell. Robots Syst.*, 1995, vol. 1, pp. 399–406.

[3] D. W. Robinson, J. E. Pratt, D. J. Paluska, and G. A. Pratt, "Series elastic actuator development for a biomimetic walking robot," in *Proc. IEEE/ASME Int. Conf. Adv. Intell. Mechatron.*, 1999, pp. 561–568.

[4] C. An and J. Hollerbach, "Dynamic stability issues in force control of manipulators," in *Proc. IEEE Int. Conf. Robot. Automat.*, 1987, vol. 4, pp. 890–896.

[5] S. Eppinger and W. Seering, "Understanding bandwidth limitations in robot force control," in *Proc. IEEE Int. Conf. Robot. Automat.*, 1987, pp. 904–909.

[6] W. S. Newman, "Stability and performance limits of interaction controllers," *J. Dynamic Syst., Meas., Control*, vol. 114, no. 4, pp. 563–570, 1992.

[7] J.W. Hurst, A. Rizzi, and D. Hobbelen, "Series elastic actuation: Potential and pitfalls," *Workshop on Morphology, Control, and Passive Dynamics, IEEE International Conference on Intelligent Robots and Systems (IROS)*, 2005.

[8] J. Oblak and Z. Matjačić, "Design of a series visco-elastic actuator for multi-purpose rehabilitation haptic device," *J. Neuroengineering Rehabil.*, vol. 8, no. 1, pp. 1–14, 2011.

[9] M. J. Kim, A. Werner, F. C. Loeffl, and C. Ott, "Enhancing joint torque control of series elastic actuators with physical damping," in *Proc. IEEE Int. Conf. Robot. Automat.*, 2017, pp. 1227–1234.

[10] U. Mengilli, Z. O. Orhan, U. Caliskan, and V. Patoglu, "Passivity of series damped elastic actuation under velocity-sourced impedance control," in *Proc. IEEE World Haptics Conf.*, 2021, pp. 379–384.

[11] C. U. Kenanoglu and V. Patoglu, "A fundamental limitation of passive spring rendering with series elastic actuation," *IEEE Trans. Haptics*, vol. 16, no. 4, pp. 456–462, Oct.–Dec. 2023.

[12] G. Wyeth, "Demonstrating the safety and performance of a velocity sourced series elastic actuator," in *Proc. IEEE Int. Conf. Robot. Automat.*, 2008, pp. 3642–3647.

[13] A. Otaran, O. Tokatli, and V. Patoglu, "Physical human-robot interaction using HandsOn-SEA: An educational robotic platform with series elastic actuation," *IEEE Trans. Haptics*, vol. 14, no. 4, pp. 922–929, Oct.–Dec. 2021.

[14] F. E. Tosun and V. Patoglu, "Necessary and sufficient conditions for the passivity of impedance rendering with velocity-sourced series elastic actuation," *IEEE Trans. Robot.*, vol. 36, no. 3, pp. 757–772, Jun. 2020.

[15] J. E. Colgate and N. Hogan, "Robust control of dynamically interacting systems," *Int. J. Control*, vol. 48, no. 1, pp. 65–88, 1988.

[16] R. B. Gillespie, D. Kim, J. M. Suchoski, B. Yu, and J. D. Brown, "Series elasticity for free free-space motion for free," in *Proc. IEEE Haptics Symp.*, 2014, pp. 609–615.

[17] F. Sergi and M. K. O'Malley, "On the stability and accuracy of high stiffness rendering in non-backdrivable actuators through series elasticity," *Mechatronics*, vol. 26, pp. 64–75, 2015.

[18] T. Horibe, E. Treadway, and R. B. Gillespie, "Comparing series elasticity and admittance control for haptic rendering," in *Proc. Haptics, Perception, Devices, Control, and Appl.*, 2016, pp. 240–250.

[19] D. P. Losey and M. K. O'Malley, "Effects of discretization on the K-Width of series elastic actuators," in *Proc. IEEE Int. Conf. Robot. Automat.*, 2017, pp. 421–426.

[20] C. U. Kenanoglu and V. Patoglu, "Passive realizations of series elastic actuation: Effects of plant and controller dynamics on haptic rendering performance," *IEEE Trans. Haptics*, vol. 17, no. 4, pp. 882–899, Oct.–Dec. 2024.

[21] E. Colgate and N. Hogan, "An analysis of contact instability in terms of passive physical equivalents," in *Proc. Int. Conf. Robot. Automat.*, 1989, vol. 1, pp. 404–409.

[22] U. Caliskan and V. Patoglu, "Efficacy of haptic pedal feel compensation on driving with regenerative braking," *IEEE Trans. Haptics*, vol. 13, no. 1, pp. 175–182, Jan.–Mar. 2020.

[23] C. U. Kenanoglu and V. Patoglu, "Passivity of series elastic actuation under model reference force control during null impedance rendering," *IEEE Trans. Haptics*, vol. 15, no. 1, pp. 51–56, Jan.–Mar. 2022.

[24] S. Haykin, *Active Network Theory*. Reading, MA, USA: Addison-Wesley, 1970.